

Research Article

Optimized Efficiency at Two Optimum Operations of a Stochastically Driven Quantum Dot Heat Engine

Yigermal Bassie¹,^{ORCID} Tibebe Birhanu,² Yoseph Abebe,³ and Mulugeta Bekele⁴

¹Department of Physics, Wolkite University, Wolkite, Ethiopia

²Department of Physics, University of Gondar, Gondar, Ethiopia

³Department of Physics, Debre Markos University, Debre Markos, Ethiopia

⁴Department of Physics, Addis Ababa University, Addis Ababa, Ethiopia

Correspondence should be addressed to Yigermal Bassie; yigermal.bassie@wku.edu.et

Received 15 March 2022; Revised 4 July 2022; Accepted 24 August 2022; Published 10 October 2022

Academic Editor: Bin Pang

Copyright © 2022 Yigermal Bassie et al. This is an open access article distributed under the Creative Commons Attribution License, which permits unrestricted use, distribution, and reproduction in any medium, provided the original work is properly cited.

We take a stochastically driven single-level quantum dot embedded between two metallic leads at different temperatures works as a heat engine. We numerically study the optimized efficiency at two optimum operations, which lies between the maximum and minimum efficiency. The minimum efficiency either takes the efficiency value at maximum power or the lowest possible value, zero. Using a unified criterion for energy converters, we find the optimum working condition for the heat engine. We study the optimized efficiency of a quantum dot heat engine according to the optimization criteria to find their corresponding optimized quantities in an external magnetic field (stochastic driving force). Accordingly, we found (1) efficiency-wise, optimized efficiency is better than efficiency at maximum power; (2) power-wise, the optimized power is smaller than its value at maximum power by 35%; and (3) period-wise, it performs the task in a cycle twice that of the period at maximum power. We study the overall performance of the heat engine by introducing a figure of merit that considers the contribution of each of the above quantities as a function of Carnot efficiency. Based on the proposed figure of merit, the model shows that the second optimization criteria are 3 times better than the first optimization criteria as a function of Carnot efficiency.

1. Introduction

The concept of thermodynamics has been developed from the analysis of heat engine performance. Carnot invented an idealized mathematical model of heat engines called the Carnot cycle and proved that there exists a maximum efficiency of all heat engines, which is given by Carnot efficiency. This efficiency is a central cornerstone of thermodynamics. It states that the efficiency of a reversible Carnot heat engine attains the maximum possible work for a given temperature of the hot reservoir, T_h , and cold reservoir, T_c . Due to an infinitely slow operation, it generates zero power. The efficiency ($\eta_c = 1 - T_c/T_h$) of the Carnot cycle is the upper bound of the efficiency at which real heat engines are unrealistically high. The practical implications are more limited since the upper limit η_c is only reached for reversible engines. One of the important questions is what will be the efficiency at a

maximum power of a system that is operating in a finite time. In a groundbreaking work, Curzon and Ahlborn [1] obtained this efficiency for the Carnot engine by optimizing the Carnot cycle with respect to power rather than efficiency, which is given by Curzon-Ahlborn efficiency, η_{CA}

$$\eta_{CA} = 1 - \sqrt{\frac{T_c}{T_h}} = \frac{\eta_c}{2} + \frac{\eta_c^2}{8} + \vartheta(\eta_c^3). \quad (1)$$

This efficiency is used to seek a more realistic upper bound on the efficiency of a heat engine in the endoreversible approximation [1, 2] (taking into account the dissipation only in the heat transfer process). Currently, it has been shown that the Curzon-Ahlborn efficiency is an exact consequence of linear irreversible thermodynamics when operating under conditions of strong coupling between the heat flux and the work

[3–5]. The value of $1/2$ for the linear coefficient in Eq. (1) is therefore universal for such systems.

Recently, efficiency at maximum power (η_{mp}) in heat engines has been reported in Refs. [3, 6–10]. In addition, the universal values for different model has been reported in Ref. [11]. There has recently been a resurgence of interest in the behavior of small systems out of equilibrium. A significant amount of research is being conducted to investigate small thermodynamic machine's efficiency at maximum output. This is motivated in part by the possible universality for systems driven by a small temperature difference [3, 6, 12]. As a result, it is worthwhile to investigate how quantum effects may influence the efficiency of devices at maximum output.

Several different optimization criteria have been proposed. However, they suffer from a lack of generality since they apply to a particular heat devices [11, 13, 14]. Among these methods, the two most often used for optimizing heat devices either require the evaluation of the entropy generation, which may be difficult for systems far from equilibrium, or depend on the parameters of the environment, which are usually difficult to determine. According to Hernandez et al. [15], the entropy generation minimization and exergy analysis are the most common ways of optimization methods. To identify the point of operation of an engine where the trade-off between energy cost and fast transport is compromised [15], this optimization criterion presents the advantage of being independent of any environment parameter and does not require the explicit evaluation of entropy generation. Besides, this method can potentially apply to a large range of engine sizes ranging from nanoscopic to macroscopic devices. Using this optimization criterion to a Brownian heat engine, they found its optimized efficiency lies between efficiency at maximum power and Carnot efficiency [16]. Moreover, results obtained from the application of this method on endoreversible Carnot-type engines agree with those obtained by applying ecological-like criteria which involve the explicit derivation of entropy generation [17].

For irreversible heat engines, it gives a performance regime lying between the maximum efficiency and the efficiency at maximum power, a regime considered optimum for traditional heat engines [14]. Besides, the optimized efficiencies of the four representative models of heat engines have been reported in Ref. [11], and they investigated their optimized efficiencies are not only larger than the efficiencies at maximum power but found them to have sort of a universal behavior.

Recently, there have been many interests in studying quantum dot heat engines. Esposito et.al. [18] proposed a model that consists of a single-level quantum dot in contact with hot and cold heat reservoirs in an external magnetic field (stochastic driving force). In a presence of thermal gradient, they studied how the device operates as a heat engine, determined the efficiency at maximum power, and compared their value with that of the Curzon-Alborn efficiency. Since it operates at maximum power, however, it wastes a large amount of the input energy though the task is accomplished in a short enough time. One can think of minimizing the wastage by appropriately relaxing the operating time. Our inspiration is to develop miniaturized devices to utilize energy conversion at the nanoscale. So,

we need to minimize the waste energy and improve such engine performance. In addition, we are motivated to know how much of the maximum available power is being utilized and how the model performs the task at the optimum condition. Recently, few papers have appeared related to quantum dot engine [19–26]. They studied efficiency, power, and period at two optimum operations of a thermoelectric single-level quantum dot in the absence of stochastic external forces. With time, researchers [27] take a single-level quantum dot embedded between two metallic leads at different temperatures and chemical potentials as a heat engine. They studied efficiency, power, and period at two optimum operations of a thermoelectric single-level quantum dot in the absence of stochastic external forces [27]. Besides, the optimized efficiency of a stochastically driven quantum dot heat engine was presented in Refs. [28, 29].

In this paper, we study the optimized efficiencies of the heat engine model, which is proposed by Esposito et al. [18]. We find the optimized efficiencies, which are bounded between the Carnot efficiency and the efficiency at maximum power. We also study the scaled electron energy barriers, power output, optimized efficiencies (η_{opt}), the ratio of optimized efficiencies to the efficiency at maximum power, i.e., efficiency-wise (ε_{opt}), the ratio of optimized power to the maximum power, i.e., optimized powers (ω_{opt}), optimized periods (τ_{opt}) which is defined as the inverse of the current from and to the quantum dot, relative efficiency η_{rel} , and relative periods τ_{rel} with different conditions. Finally, by applying optimization criteria, we define a figure of merit to quantify how the engine operates under any condition.

The rest of this paper is organized as follows: in Section 2, the model of the system is presented, and the thermodynamics quantities are determined. In Section 3, we discuss the maximum power output of the model with different parameters. In Section 4, we find and analyze the model's performance characteristics. Section 5 deals with the summary.

2. Theory and Model

We consider a particular model that consists of a single-level quantum dot in contact with hot left lead, temperature T_L , and chemical potential μ_L , and with cold right lead, temperature T_R , and chemical potential μ_R in an external magnetic field (stochastic driving force) (see in Figure 1).

In the presence of an external magnetic field, the system's energy level stochastically switched between an upper and a lower energy value, ε_j , respectively, where $j = u, d$. The upward and downward rates are k^+ and k^- . In each energy level; we have two possible energy states of the system, either empty or occupied. The system's possible energy states are denoted by j_n , where $n = 0, 1$ denotes an empty or occupied energy state, respectively. Therefore, we have four possible states of the system such as u_1, u_0, d_1, d_0 . The evolution of the occupation probability of the system state is described by the stochastic master equation in terms of $k_j^\pm = k_{Lj}^\pm + k_{Rj}^\pm$; the total transition rate out of the dot (+) or into the dot (-) of either lead is given by [18, 30, 31]

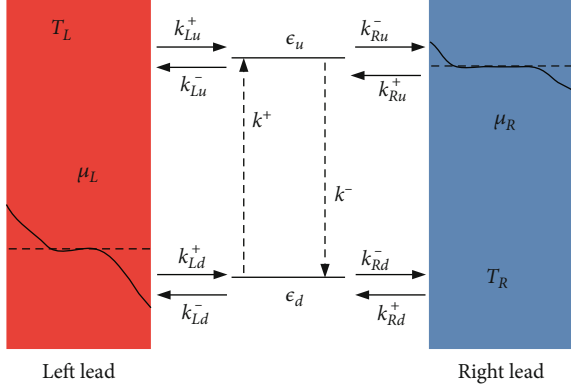


FIGURE 1: The model of a stochastically driven quantum dot heat engine. The arrows show all possible transitions.

$$\frac{d}{dt} \begin{pmatrix} P_{u1} \\ P_{u0} \\ P_{d1} \\ P_{d0} \end{pmatrix} = M \begin{pmatrix} P_{u1} \\ P_{u0} \\ P_{d1} \\ P_{d0} \end{pmatrix}, \quad (2)$$

with

$$M = \begin{pmatrix} -k^- - k_u^- & k_u^+ & k^+ & 0 \\ k_u^- & -k^- - k_u^- & 0 & k^+ \\ k^- & 0 & -k^+ - k_d^+ & k_d^+ \\ 0 & k^- & k_d^- & -k^+ - k_d^+ \end{pmatrix}, \quad (3)$$

where $P_{jn}(t)$ is the occupation probability of finding the system in state j at time t with the corresponding electron number $n = 0, 1$. The transition rates of an electron into lead ν , where $\nu = L, R$, from the dot, and out of lead ν to the dot, are given, respectively, by $k_{\nu j}^- = \Gamma_{\nu j}(1 - f_{\nu j})$ and $k_{\nu j}^+ = \Gamma_{\nu j}f_{\nu j}$. The expression $f_{\nu j} = [\text{Exp}\{\varepsilon_j - \mu_{\nu}/T_{\nu}\} + 1]^{-1}$ is the Fermi distribution in lead ν , and $\Gamma_{\nu j}$ is the coupling strength between the lead and the dot in state j .

The crucial variables of the problem are the right and the left scaled electron energy barriers (with $k_B = 1$), which are given, respectively, by

$$x_R = \frac{\varepsilon_u - \mu_R}{T_R}, \quad (4)$$

$$x_L = \frac{\varepsilon_d - \mu_L}{T_L}. \quad (5)$$

The probability currents between the four states are $I_{un \leftarrow dn} = k^+ P_{dn} - k^- P_{un}$ and $I_{j1 \leftarrow j0}^{\nu} = k_{\nu j}^+ P_{j0} - k_{\nu j}^- P_{j1}$. It is convenient to introduce the total current to the dot when it is down or up is given by the sum $I_{j1 \leftarrow j0} = \sum_{\nu} I_{j1 \leftarrow j0}^{\nu}$. In the steady state, using Eq. (2), we easily solve the occupation probabilities, and the average currents entering the system

from the hot reservoir are equal to that entering the cold reservoir from the system. Therefore, the energy current injected into the system by the stochastic driving can be expressed as

$$I_{\text{ext}} = (\varepsilon_u - \varepsilon_d)I_{u1 \leftarrow d1} = (\varepsilon_u - \varepsilon_d)I, \quad (6)$$

while the matter (M) and energy (E) currents entering the system from lead ν are given by

$$I_M^{\nu} = \sum_j I_{j1 \leftarrow j0}^{\nu} \text{ and } I_E^{\nu} = \sum_j \varepsilon_j I_{j1 \leftarrow j0}^{\nu}. \quad (7)$$

In steady state, heat flux extracted from the lead ν is given by

$$\dot{Q}^{\nu} = I_E^{\nu} - \mu_{\nu} I_M^{\nu}. \quad (8)$$

with satisfies matter $I_M^L = -I_M^R$ and energy $I_{\text{exe}} = -I_E^L - I_E^R$ conservation at steady state.

Therefore, the power becomes

$$P = -\sum_{\nu} \dot{Q}^{\nu} = (\varepsilon_u - \varepsilon_d)I + (\mu_R - \mu_L)I_M^L, \quad (9)$$

which is the contribution of the energy flux injected by the stochastic driving and the energy flux required to bring an electron from the left lead through the dot to the right lead.

The heat flux entering from the left lead to the device and the power performed by the device upon bringing electron from the left lead to the right lead is given by Eqs. (8) and (9), respectively. The corresponding efficiency of the model is given by

$$\eta = 1 - \frac{x_R}{x_L}(1 - \eta_C), \quad (10)$$

where the isothermal operation of our engine can be operated under more conventional operating conditions.

3. The Efficiency at Maximum Power

In this section, we consider a model that is consisting of a single level quantum dot in contact with hot and cold heat reservoirs in an external magnetic field [18]. In the presence of thermal gradient, they studied that the device operate as a heat engine, described the efficiency at maximum power of the model in the tight coupling regime, and compared their value with that of the Curzon-Alborn efficiency. Besides, they also found numerical solutions for maximum electron energy barriers and power output of the device. In the tight coupling regime, the power output of the model can be written as

$$P = T_L(x_L - x_R)(1 - \eta_C)I(x_L, x_R). \quad (11)$$

To obtain the efficiency at maximum power, the power output takes its maximum value when $\partial P / \partial x_L|_{x_L^{mp}} = 0 = \partial P / \partial x_R|_{x_R^{mp}}$. In the extreme conditions, and the

expression of the right electron energy barrier and left electron energy barrier is given by

$$x_R^{mp} = 2 \ln \left[\frac{\cosh(x_L^{mp}/2)}{\sqrt{1-\eta_c}} + \sqrt{\frac{\cosh^2(x_L^{mp}/2)}{1-\eta_c} - 1} \right], \quad (12)$$

$$x_L^{mp} + 2(\eta_c - 1) \ln \left[\frac{\cosh(x_L^{mp}/2)}{\sqrt{1-\eta_c}} + \sqrt{\frac{\cosh^2(x_L^{mp}/2)}{1-\eta_c} - 1} \right] - \sqrt{2} \cosh\left(\frac{x_L^{mp}}{2}\right) \sqrt{\cosh(x_L^{mp}) + 2\eta_c - 1 + \sinh(x_L^{mp})} = 0, \quad (13)$$

respectively.

As a starting point, we solve the numerical solutions for the scaled electron energy barriers at maximum power condition, as shown in Figure 2. To round out the picture, we show in Figure 2 the numerical solutions for right, x_R^{mp} (the blue solid line), and left, x_L^{mp} (the blue dotted line) electron energy barriers as functions of Carnot efficiency (η_c). We have seen that the left electron energy barrier x_L^{mp} is always of order unity so that the regime of maximum power cannot be well described by either a high- or a low-temperature expansion. It can also be seen that the maximum power is a monotonically increasing function of η_c .

Due to their technological importance, we also give the corresponding maximum power and operational conditions of the scaled energies.

Figure 3 depicts the performance characteristic of the power output versus Carnot efficiency at maximum power with different condition. We demonstrated that the difference between the lowest and highest maximum power as a function of Carnot efficiency (blue line) is due to its monotonic increase by increasing the Carnot efficiency. This numerical finding is assisted by examining the behavior of output powers in Figure 3, where the power output strongly depends on reservoir temperature choices.

The transcendental equation can be solved perturbatively for small Carnot efficiency, which is given by

$$\eta_{mp} = \frac{\eta_c}{2} + \frac{\eta_c^2}{8} + \vartheta\eta_c^3. \quad (14)$$

We thus recover the universal value $\eta_c/2$ in the linear regime [3], as well as the factor 1/8 for the quadratic coefficient [6]. This result obtained in Eq. (14) meets with the work of [7]. Here, we can see that the coefficient of the linear and the quadratic terms agrees with that of the Curzon-Ahlborn model had been reported in [18].

We also numerically solve the efficiency at maximum power displayed in Figure 4. We note that the efficiency at maximum power increases monotonically when driven out of equilibrium. It is bounded from above by Carnot efficiency η_c , while the Curzon-Ahlborn efficiency η_{CA} provides a rather tight lower bound. When a system operating at maximum power condition wastes a large amount of the

input energy even if the task is accomplished in a short enough time. In the next section, we obtain the device's optimal performance under two operational conditions by appropriately relaxing the operating time.

4. Optimized Efficiency at Two Optimum Operations

In this section, we study the performance of a heat engine both theoretically and numerically. Using a unified criterion for energy converters, we derive the expression for the optimized scaled electron energy barriers, optimized efficiencies (η_{opt}), efficiency-wise (ϵ_{opt}), optimized powers (ω_{opt}), optimized periods (τ_{opt}), relative efficiency η_{rel} , and relative periods τ_{rel} for two cases. Besides, we quantify the overall performance of the heat engine by introducing a figure of merit.

The optimized efficiencies of the heat engine can be obtained by defining the rate of objective function ($\dot{\Omega}$). Then, the rate of objective function can be defined as the difference between effective useful power $\dot{E}_{u,eff} = (\eta - \eta_{min})\dot{Q}_{in}$ and lost useful power $\dot{E}_{u,lost} = (\eta_{max} - \eta)\dot{Q}_{in}$ quantities, where \dot{Q}_{in} is the input power. An engine operating in a finite time has efficiency its laying between the minimum efficiency, η_{min} , and maximum efficiency, η_{max} , i.e., $\eta_{min} \leq \eta \leq \eta_{max}$. The rate of objective function can be described as the difference between two quantities ($\dot{E}_{u,eff} - \dot{E}_{u,lost}$),

$$\dot{\Omega} = (2\eta - \eta_{min} - \eta_{max})\dot{Q}_{in}. \quad (15)$$

These two quantities are functions of independent and dependent parameters describing the process. Then to find the system's optimized efficiencies, first, we need to find the maximum value of the rate of objective function with respect to the system's set of control parameters. In the rate of objective functions, the minimum efficiency takes the efficiency value at maximum power (η_{mp}), and the maximum efficiency takes the Carnot efficiency, η_c (hereafter referred to as case 1). This case considers the whole possible range to search for optimization. The rate of objective function for case 1 is then given by

$$\dot{\Omega}_1 = (2\eta - \eta_{mp} - \eta_c)\dot{Q}_{in}, \quad (16)$$

where the input power of the model $\dot{Q}_{in} = T_L x_L \alpha(f(x_L) - f(x_R))$. Here, $f(x_L)$ and $f(x_R)$ are the left and right lead Fermi distribution, respectively.

On the other hand, the minimum efficiency takes the lowest possible value (i.e., $\eta_{min} = 0$), and the maximum efficiency takes the Carnot efficiency (i.e., $\eta_{min} = \eta_c$) (hereafter referred to as case 2). In this case rate of the objective function can be described as

$$\dot{\Omega}_2 = (2\eta - \eta_c)\dot{Q}_{in}. \quad (17)$$

In order to maximize the rate of objective function with respect to the right and left electron energy barriers, we need

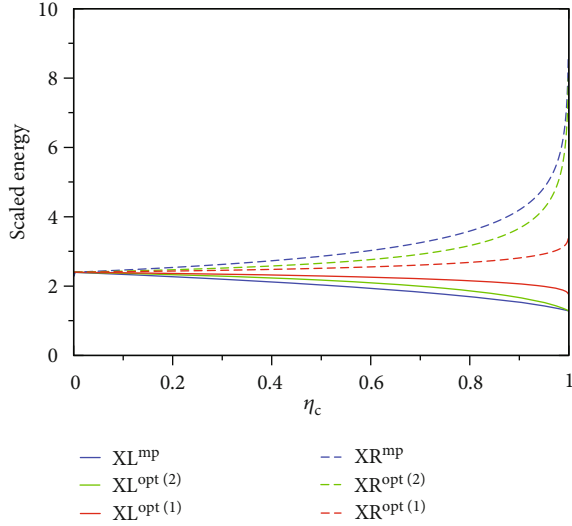


FIGURE 2: (Color online) Scaled electron energy barriers x_L at maximum power and at the two optimization criteria condition, and the dotted line represents the corresponding (scaled) energy x_R at maximum power and at the two cases of optimization criteria condition as a function of the Carnot efficiency $\eta_c = 1 - T_R/T_L$.

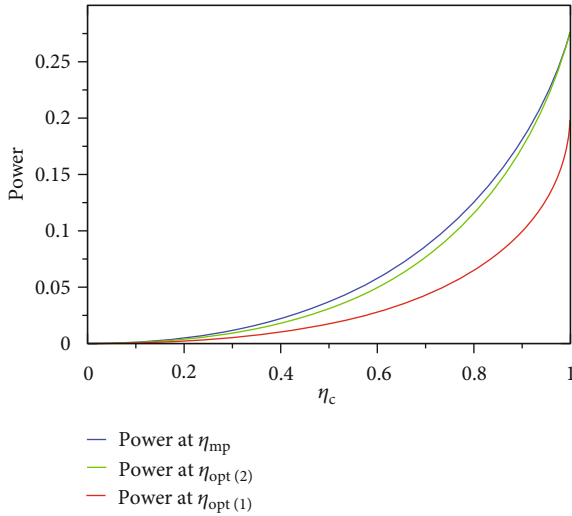


FIGURE 3: Power output versus η_c at maximum power and two cases of optimization criteria condition.

to solve $\partial \dot{\Omega} / \partial x_R|_{x_R^{\text{opt}}} = 0 = \partial \dot{\Omega} / \partial x_L|_{x_L^{\text{opt}}}$. In the optimal conditions, the expression of the right electron energy barrier and left electron energy barrier can be expressed base on the two cases.

The optimized efficiency (in the first case described in Eq. (16)), the rate of objective function takes its maximum value when $\partial \dot{\Omega}_1 / \partial x_R|_{x_R^{\text{opt}}} = 0 = \partial \dot{\Omega}_1 / \partial x_L|_{x_L^{\text{opt}}}$. In these conditions, the expression of the right electron energy barrier and left electron energy barrier is given by

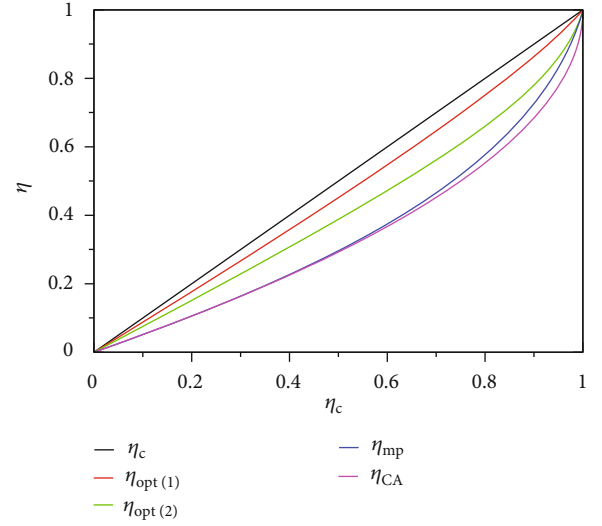


FIGURE 4: Plot of efficiency at maximum power (blue line); at optimized power efficiency when ($\eta_{\text{min}} = \eta_{\text{mp}}$) (red line); at optimized efficiency when ($\eta_{\text{min}} = 0$) (green); at Carnot efficiency (black) and Curzon Ahlborn efficiency (magenta line) versus η_c .

$$x_R^{\text{opt}(1)} = 2 \ln \left[\sqrt{\frac{2 - \eta_{\text{mp}} - \eta_c}{2\eta_c - 2}} \cosh \left(\frac{x_L^{\text{opt}(1)}}{2} \right) + \sqrt{\frac{2 - \eta_{\text{mp}} - \eta_c}{2\eta_c - 2} \cosh^2 \left(\frac{x_L^{\text{opt}(1)}}{2} \right) - 1} \right], \quad (18)$$

$$x_L^{\text{opt}(1)} + \frac{4(\eta_c - 1)}{2 - \eta_{\text{mp}} - \eta_c} \ln \left[\sqrt{\frac{2 - \eta_{\text{mp}} - \eta_c}{2 - 2\eta_c}} \cosh \left(\frac{x_L^{\text{opt}(1)}}{2} \right) + \sqrt{\frac{2 - \eta_{\text{mp}} - \eta_c}{2 - 2\eta_c} \cosh^2 \left(\frac{x_L^{\text{opt}(1)}}{2} \right) - 1} \right] + \sinh \left(x_L^{\text{opt}(1)} \right) - \sqrt{2} \cosh \left(\frac{x_L^{\text{opt}(1)}}{2} \right) \cdot \sqrt{\cosh \left(x_L^{\text{opt}(1)} \right) + \frac{3\eta_c - \eta_{\text{mp}} - 2}{2 - \eta_{\text{mp}} - \eta_c}} = 0, \quad (19)$$

respectively. The above equations are transcendental, so we solve numerically and displayed in Figures 2 and 3. It shows the cure of first case of optimization criteria in the form of the scaled energy and output power as a function of Carnot efficiency (red line). In both Figures 3 and 4, the difference between the lowest and largest output power is due to its monotonic increasing by raising the Carnot efficiency. Such a numerical finding is assisted by examining the behavior of output powers in Figure 3, in which the power output strongly depends on the reservoir's temperature choices.

The power series expansion of optimized efficiency in the limit of small Carnot efficiency, η_c for the first case of optimization scenarios, which are given by

$$\eta_{\text{opt}(1)} = 0.875\eta_c + 0.03875\eta_c^2 + \vartheta(\eta_c^3). \quad (20)$$

For the first case of optimized efficiency (Eq. (20)), which is identical to [27] in the linear regime. On the other hand, we solve the optimized efficiency of the model numerically, as shown in Figure 4 (red line). We note that the optimized efficiency increases monotonically when driven out of equilibrium. It is bounded from above by Carnot efficiency η_c , while the efficiency at maximum power η_{mp} provides a rather tight lower bound. Using the corresponding expression for the input power (\dot{Q}_{in}), efficiency (η), and efficiency at maximum power (η_{mp}) of the model, we obtain the values of scaled physical quantities such as the efficiency-wise ($\varepsilon_{\text{opt}} = \eta_{\text{opt}}/\eta_{mp}$), optimized power ($\omega_{\text{opt}} = P_{\text{opt}}/P_{mp}$), and optimized period ($\tau_{\text{opt}} = \pi_{\text{opt}}/\pi_{mp}$). These scaled physical quantities in the first case of optimization scenarios can be expressed as

$$\varepsilon_{\text{opt}(1)} = \frac{7}{4} - \frac{9}{25}\eta_c - \vartheta(\eta_c^2), \quad (21)$$

$$\omega_{\text{opt}(1)} = \frac{7}{16} + \frac{3}{16}\eta_c + \vartheta(\eta_c^2), \quad (22)$$

$$\tau_{\text{opt}(1)} = 4 - \frac{1}{2}\eta_c - \vartheta(\eta_c^2), \quad (23)$$

respectively. These scaled quantities are expressed in a series expansion in the small η_c limit.

Similarly, optimized efficiency (in the function case described in Eq. (17)), the rate of objective function takes its maximum value when $\partial\dot{\Omega}_2/\partial x_R|_{x_R^{\text{opt}}} = 0 = \partial\dot{\Omega}_2/\partial x_L|_{x_L^{\text{opt}}}$. In this conditions, the expression of the right electron energy barrier and left electron energy barrier is given by

$$x_R^{\text{opt}(2)} = 2 \ln \left[\sqrt{\frac{2-\eta_c}{2\eta_c-2}} \cosh\left(\frac{x_L^{\text{opt}(2)}}{2}\right) + \sqrt{\frac{2-\eta_c}{2\eta_c-2}} \cosh^2\left(\frac{x_L^{\text{opt}(2)}}{2}\right) - 1 \right], \quad (24)$$

$$x_L^{\text{opt}(2)} + \sinh\left(x_L^{\text{opt}(2)}\right) + \frac{4(\eta_c-1)}{2-\eta_c} \ln \left[\sqrt{\frac{2-\eta_c}{2-2\eta_c}} \cosh\left(\frac{x_L^{\text{opt}(2)}}{2}\right) + \sqrt{\frac{2-\eta_c}{2-2\eta_c}} \cosh^2\left(\frac{x_L^{\text{opt}(2)}}{2}\right) - 1 \right] - \sqrt{2} \cosh\left(\frac{x_L^{\text{opt}(2)}}{2}\right) \sqrt{\cosh\left(x_L^{\text{opt}(2)}\right) + \frac{3\eta_c-2}{2-\eta_c}} = 0. \quad (25)$$

The resulting transcendental equations can be solved numerically and displayed in Figures 2 and 3. These figures proved the cure of the second case of optimization criteria in the form of the scaled energy and output power as a function of Carnot efficiency (green line). Figures 3 and 4 are exploits the difference between the lowest and largest output

power is due to its monotonically increase by raising the Carnot efficiency. Such a numerical finding is assisted by examining the behavior of output powers in Figure 3, in which the power output strongly depends on the reservoirs' temperature choices.

In the second case of optimization scenario, to obtain the power series expansion of optimized efficiency in the limit of small Carnot efficiency, η_c is given by

$$\eta_{\text{opt}(2)} = 0.75\eta_c + 0.03125\eta_c^2 + \vartheta(\eta_c^3). \quad (26)$$

The expression of the optimized efficiency for the second case (Eq.(26)) is identical to in the linear regime [11] for the particular model they studied. On the other hand, we numerically solve the optimized efficiency of the second case as shown in Figure 4 (green line). Figure 4 (green line) depicts that the optimized efficiency increases monotonically and approaching to one. It is bounded between the first case of optimized efficiency and the efficiency at maximum power. Using the same approach as in the first case, the value of scaled quantities in the second case of the optimization scenario can be expressed as

$$\varepsilon_{\text{opt}(2)} = \frac{3}{2} - \frac{5}{16}\eta_c - \vartheta(\eta_c^2), \quad (27)$$

$$\omega_{\text{opt}(2)} = \frac{3}{4} + \frac{1}{8}\eta_c + \vartheta(\eta_c^2), \quad (28)$$

$$\tau_{\text{opt}(2)} = 2 - \frac{1}{2}\eta_c - \vartheta(\eta_c^2), \quad (29)$$

in a series expansion in the limit of small η_c .

In both cases of optimization scenarios under consideration, our optimized efficiency results of the particular model have a similar results to Ref. [27].

From Figure 4, we note that as Carnot efficiency goes to zero, the optimized efficiency goes to zero. This is because when Carnot efficiency becomes very small (i.e., as the temperature of the two leads approaches the same), the heat flux that is getting into the quantum dot becomes very small; hence, the optimized efficiency approaches zero, whereas Carnot efficiency approaches one (i.e., as the temperature of the two leads are different), the optimized efficiency approaches to one.

Figure 5 shows the numerical solutions for the ratio of optimized efficiency for the two cases of optimization criteria to the efficiency at maximum power versus the full range of Carnot efficiency. We can see that as Carnot efficiency approaches to one, ε_{opt} monotonically decreases and reaches the same value. This numerical solution illustrates that the first optimization is more efficient than the second optimization overall range of η_c . However, this advantage is more pronounced for smaller values of Carnot efficiency.

Figure 6 compares how much of the maximum available power is utilized by the two optimization criteria. The figure clearly shows that the first case of the optimization criterion utilizes a large amount of maximum power at a small value of Carnot efficiency and performs even better as Carnot

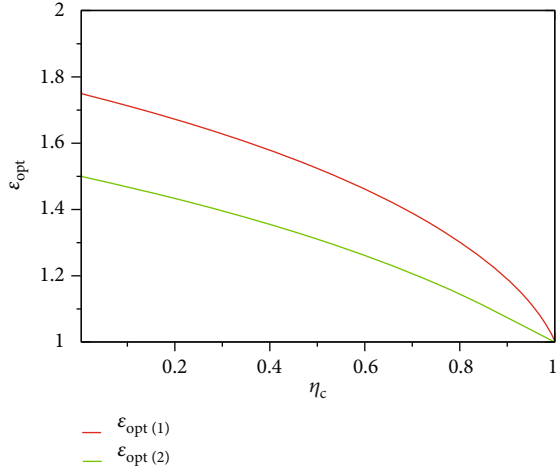


FIGURE 5: The numerical values of the ratio of optimized efficiency for the two cases of optimization criteria to the efficiency at maximum power versus the Carnot efficiency.

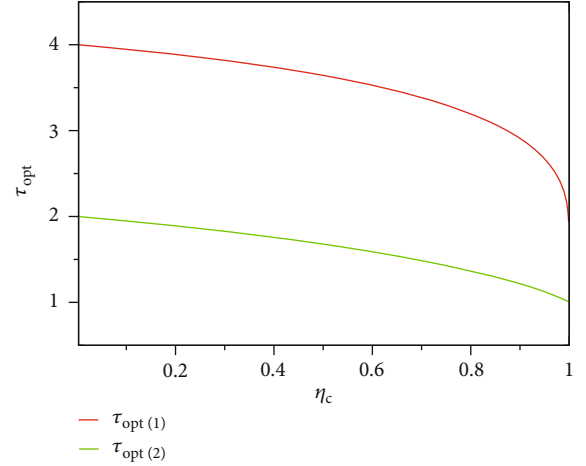


FIGURE 7: The ratio of optimized period for the two cases of optimization criteria to the period at maximum power versus the Carnot efficiency.

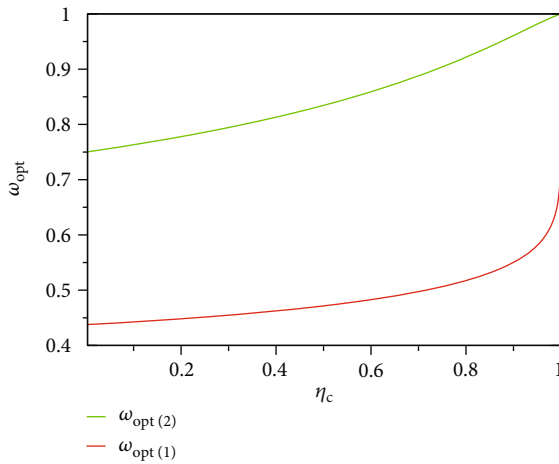


FIGURE 6: The numerical values of the ratio of optimized power for the two cases of optimization criteria to the maximum power versus the Carnot efficiency.

efficiency approaches one. The second case of optimization, on the other hand, is less than half of the maximum available power over the entire range of Carnot efficiency.

As we see from Figure 7, the Carnot efficiency approaches its maximum value, and the time it takes to complete its work decreases monotonically in both cases of optimization criterion. However, as the Carnot efficiency approaches zero, the time required to complete the task increases monotonically in both cases. The figure clearly shows that in the limit of small Carnot efficiency, the second optimization criterion completes its task in a cycle twice as long as the period at maximum power. The first optimization criterion, on the other hand, performs its tasks at a rate ranging from two and a quarter to four times that of the maximum power period over the entire range of η_c .

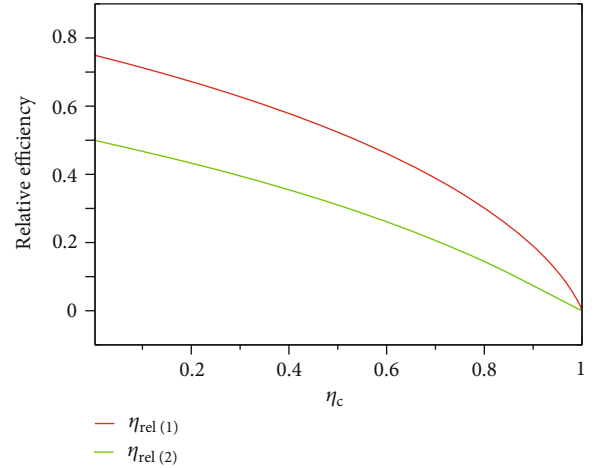


FIGURE 8: The relative efficiency ($\eta_{rel} = \eta_{opt} - \eta_{mp}/\eta_{mp}$) of the two cases of optimization criteria versus Carnot efficiency.

In Figure 8, we plot the relative efficiency (η_{rel}) of the two cases of optimization criteria as a function of Carnot efficiency. When η_c goes to zero, the relative efficiency is maximum because the deviation of the two efficiencies is highest for small temperature difference. When η_c increases, relative efficiency (η_{rel}) decreases since the deviation between the two efficiencies decreases: the optimized efficiency and efficiency at maximum power get closer and closer to each other. When η_c going to maximum values-unity, the authors declare that they have no known competing financial interests. The relative efficiency becomes zero because of both the optimized efficiency and efficiency at maximum power approach to one; hence, the difference becomes zero.

Figure 9 shows the relative time, τ_{rel} , as a function of η_c that describes the relative time decreases as η_c increases in both cases of optimization criteria. This is because when the temperature of the two heat reservoirs is close to each other (i.e., when η_c is near to zero), the two cases of optimization criteria period $\tau_{op(1/2)}$ and τ_{mp} (where $\tau_{op(1/2)} > \tau_{mp}$) have maximum value,

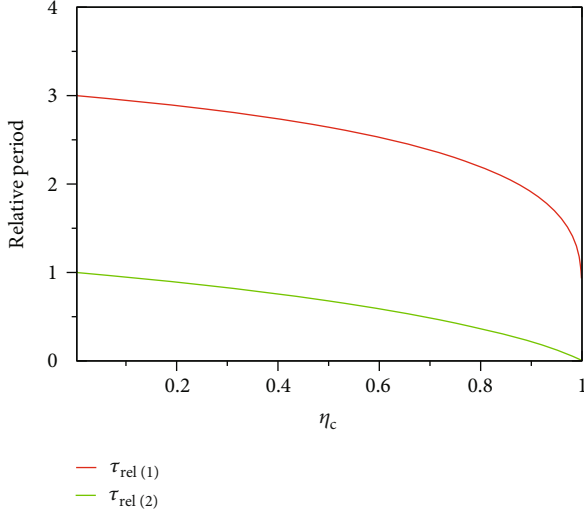


FIGURE 9: The relative period ($\tau_{\text{rel}} = \tau_{\text{opt}} - \tau_{\text{mp}}/\tau_{\text{mp}}$) of the two cases of optimization criteria versus Carnot efficiency.

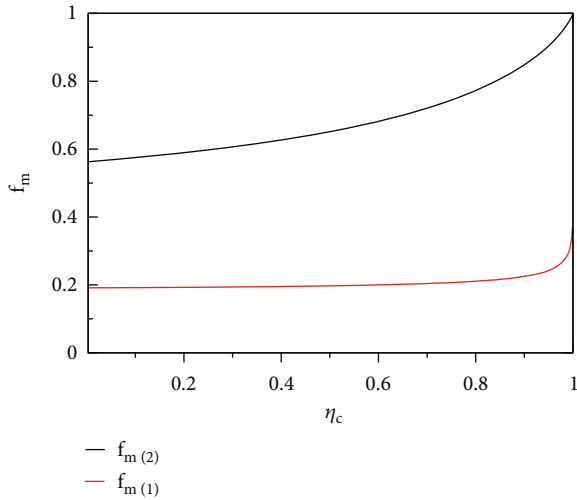


FIGURE 10: The figure of merit for the two cases of optimization criteria versus the Carnot efficiency.

their difference is large, and this decreases as η_c increases because the difference between $\tau_{\text{op}(1/2)}$ and τ_{mp} decreases.

The engine performs better in terms of efficiency-wise when subjected to the first optimization criterion than when subjected to the second criterion (Figure 5). However, when the second optimization criterion is used, the engine performs better in terms of both power-wise and period-wise than when the first optimization criterion is used (Figures 6 and 7). We introduce a figure of merit ($f_m = \varepsilon\omega/\tau$) that uses the three quantities to determine which optimization criterion provides the best trade-off.

Figure 10 shows the figure of merit for the two cases of optimization criteria versus the Carnot efficiency. Both plots increase monotonically when Carnot efficiency increase. Comparing the plot based on the optimization criteria (scenarios) clearly shows that the first optimization performs better over the second for the whole range of Carnot effi-

ciency. We see that the first optimization performs three times better than the second.

5. Summary

We considered a stochastically driven single-level quantum dot in contact between two (hot and cold) heat reservoirs. We studied the engine's performance by applying the two optimization scenarios. By applying the optimization criteria, we have found an optimized efficiency which lies between the efficiency at maximum power (and also Curzon-Ahlborn [[1]]) and maximum efficiency (Carnot efficiency). When the temperatures of the hot and cold reservoirs are close to each other, the efficiency at maximum power is $0.5\eta_c$. Using the optimization criteria, we found the optimized efficiency takes $0.875\eta_c$ and $0.75\eta_c$ values when the minimum efficiencies are $0.5\eta_c$ and zero, respectively. According to the two optimization scenarios, the first optimization is more advantageous than the second case of optimization criterion overall range of η_c . However, this advantage is more pronounced for smaller η_c , but it shrinks to the same value when η_c goes to one. Power-wise, the second optimization criterion is more advantageous than the first case of optimization criterion because the second case of optimization criterion utilizes a large amount of maximum power at a small value of Carnot efficiency and performs even better as Carnot efficiency goes to one. The second optimization criterion performs its task in a short period than that of the first optimization criterion. The overall performance of the second optimization criterion is three times better than the first one.

Data Availability

This manuscript has no associated data or the data will not be deposited.

Conflicts of Interest

The authors declare no conflicts of interest.

Authors' Contributions

YB and MB did the conception and design of study. YB performed the analytic calculations. YB and TB performed the numerical simulations. YB, TB, YA, and MB did the analysing and interpreting of the results. YB, TB, YA, and MB drafted manuscript preparation. All authors review the results and approved the final version of the manuscript.

Acknowledgments

YB would like to thank Wolkite University for material supporting to write this manuscript. We would like to thank The International Science Programme, Uppsala University, Uppsala, Sweden, for the support they have provided to our research group.

References

- [1] F. L. Curzon and B. Ahlborn, "Efficiency of a Carnot engine at maximum power output," *American Journal of Physics*, vol. 43, no. 1, pp. 22–24, 1975.
- [2] H. B. Callen, *Thermodynamics and an Introduction to Thermostatistics*, John Wiley & sons, 2nd edition, 1985.
- [3] C. Van den Broeck, "Thermodynamic efficiency at maximum power," *Physical Review Letters*, vol. 95, no. 19, article 190602, 2005.
- [4] B. J. De Cisneros and A. C. Hernández, "Collective working regimes for coupled heat engines," *Physical Review Letters*, vol. 98, no. 13, article 130602, 2007.
- [5] A. Gomez-Marin and J. M. Sancho, "Tight coupling in thermal Brownian motors," *Physical Review E*, vol. 74, no. 6, article 062102, 2006.
- [6] M. Esposito, K. Lindenberg, and C. Van den Broeck, "Universality of efficiency at maximum power," *Physical Review Letters*, vol. 102, no. 13, article 130602, 2009.
- [7] M. Esposito, R. Kawai, K. Lindenberg, and C. Van den Broeck, "Efficiency at maximum power of low-dissipation Carnot engines," *Physical Review Letters*, vol. 105, no. 15, article 150603, 2010.
- [8] M. Esposito, K. Lindenberg, and C. Van den Broeck, "Thermoelectric efficiency at maximum power in a quantum dot," *EPL (Europhysics Letters)*, vol. 85, no. 6, p. 60010, 2009.
- [9] Z. Tu, "Efficiency at maximum power of Feynman's ratchet as a heat engine," *Journal of Physics A: Mathematical and Theoretical*, vol. 41, no. 31, article 312003, 2008.
- [10] M. Esposito, "Stochastic thermodynamics under coarse graining," *Physical Review E*, vol. 85, no. 4, article 041125, 2012.
- [11] N. Sanchez-Salas, L. López-Palacios, S. Velasco, and A. C. Hernández, "Optimization criteria, bounds, and efficiencies of heat engines," *Physical Review E*, vol. 82, no. 5, article 051101, 2010.
- [12] T. Schmiedl and U. Seifert, "Efficiency at maximum power: an analytically solvable model for stochastic heat engines," *EPL (Europhysics Letters)*, vol. 81, no. 2, p. 20003, 2008.
- [13] C. Wu, *Recent Advances in Finite-Time Thermodynamics*, Nova Science Publishers, 1999.
- [14] J. Chen, "The maximum power output and maximum efficiency of an irreversible Carnot heat engine," *Journal of Physics D: Applied Physics*, vol. 27, no. 6, pp. 1144–1149, 1994.
- [15] A. C. Hernández, A. Medina, J. M. Roco, J. A. White, and S. Velasco, "Unified optimization criterion for energy converters," *Physical Review E*, vol. 63, no. 3, article 037102, 2001.
- [16] M. Asfaw and M. Bekele, "Current, maximum power and optimized efficiency of a Brownian heat engine," *The European Physical Journal B-Condensed Matter and Complex Systems*, vol. 38, no. 3, pp. 457–461, 2004.
- [17] F. Angulo-Brown, "An ecological optimization criterion for finite-time heat engines," *Journal of Applied Physics*, vol. 69, no. 11, pp. 7465–7469, 1991.
- [18] M. Esposito, N. Kumar, K. Lindenberg, and C. Van den Broeck, "Stochastically driven single-level quantum dot: a nanoscale finite-time thermodynamic machine and its various operational modes," *Physical Review E*, vol. 85, no. 3, article 031117, 2012.
- [19] Y. Liu, X. Yang, X. Hong, M. Si, F. Chi, and Y. Guo, "A high-efficiency double quantum dot heat engine," *Applied Physics Letters*, vol. 103, no. 9, article 093901, 2013.
- [20] P. A. Erdman, F. Mazza, R. Bosisio, G. Benenti, R. Fazio, and F. Taddei, "Thermoelectric properties of an interacting quantum dot based heat engine," *Physical Review B*, vol. 95, no. 24, article 245432, 2017.
- [21] M. Josefsson, A. Svilans, A. M. Burke et al., "A quantum-dot heat engine operating close to the thermodynamic efficiency limits," *Nature Nanotechnology*, vol. 13, no. 10, pp. 920–924, 2018.
- [22] M. Josefsson, A. Svilans, H. Linke, and M. Leijnse, "Optimal power and efficiency of single quantum dot heat engines: theory and experiment," *Physical Review B*, vol. 99, no. 23, article 235432, 2019.
- [23] W. Liu, L. Bai, and R. Zhang, "Optically manipulating thermodynamic performances of a quantum-dot heat engine," *Superlattices and Microstructures*, vol. 145, article 106625, 2020.
- [24] J. Du, W. Shen, X. Zhang, S. Su, and J. Chen, "Quantum-dot heat engines with irreversible heat transfer," *Physical Review Research*, vol. 2, no. 1, article 013259, 2020.
- [25] K. H. Jong, S. M. Ri, and C. W. Ri, "Parametric study for optimal performance of Coulomb-coupled quantum dots," *Journal of Physics: Condensed Matter*, vol. 33, no. 37, article 375302, 2021.
- [26] J. Um, K. E. Dorfman, and H. Park, "Coherence-enhanced quantum-dot heat engine," *Physical Review Research*, vol. 4, no. 3, 2022 <https://arxiv.org/abs/2111.09582>.
- [27] F. Borga, M. Bekele, Y. B. Tatek, and M. Tsige, "Efficiency, power, and period at two optimum operations of a thermoelectric single-level quantum dot," *Physical Review E*, vol. 86, no. 3, article 032106, 2012.
- [28] Y. B. Yassabie, *Optimized Efficiency of a Stochastically Driven Quantum Dot Heat Engine*, Ph. D. thesis, Addis Ababa University, Addis Ababa, 2012.
- [29] N. Kumar, S. Kaur, R. Kumar et al., "Interactions and competitive adsorption at solid/liquid interface," *Bulletin of the American Physical Society*, vol. 65, 2020.
- [30] U. Harbola, M. Esposito, and S. Mukamel, "Quantum master equation for electron transport through quantum dots and single molecules," *Physical Review B*, vol. 74, no. 23, article 235309, 2006.
- [31] E. Bonet, M. M. Deshmukh, and D. Ralph, "Solving rate equations for electron tunneling via discrete quantum states," *Physical Review B*, vol. 65, no. 4, article 045317, 2002.